

# Atomic Bloch-Zener Oscillations and Stückelberg Interferometry in Optical Lattices

Sebastian Kling,<sup>\*</sup> Tobias Salger, Christopher Grossert, and Martin Weitz

*Institut für Angewandte Physik der Universität Bonn, Wegelerstr. 8, 53115 Bonn*

(Dated: November 5, 2018)

## Abstract

We report on experiments investigating quantum transport and band interferometry of an atomic Bose-Einstein condensate in an optical lattice with a two-band miniband structure, realized with a Fourier-synthesized optical lattice potential. Bloch-Zener oscillations, the coherent superposition of Bloch oscillations and Landau-Zener tunneling between the two bands are observed. When the relative phase between paths in different bands is varied, an interference signal is observed, demonstrating the coherence of the dynamics in the miniband system. Measured fringe patterns of this Stückelberg interferometer allow to interferometrically map out the band structure of the optical lattice over the full Brillouin zone.

PACS numbers: 03.75.Dg, 37.10.Jk, 67.85.Hj

---

<sup>\*</sup> kling@iap.uni-bonn.de

Transport properties of a quantum object in a periodic potential are crucially determined by the particle's band structure [1]. For example, Bloch oscillations, in which a particle subjected to a uniform force in a periodic potential performs an oscillatory rather than a uniformly accelerated motion, can be well described by the dynamics within a single band of the Bloch spectrum [2, 3]. For systems with two bands energetically separated from energetic higher bands (miniband structure), as can be realized by imposing a superlattice structure onto a usual sinusoidal lattice potential, Bloch-Zener oscillations, a characteristic sequence of Bloch-oscillations and Landau-Zener transitions, have been predicted to occur when a constant force is applied [4, 5]. The avoided crossing between the two minibands can furthermore act as a coherent beam splitter when partial Landau-Zener tunneling between the subbands occurs. When an avoided crossing is used first to coherently split up and subsequently to recombine atomic wavepackets, we expect to be able to observe an interference pattern, which is analogous to the Stückelberg oscillations long known in collisional atomic physics [6, 7]. Experimentally, Bloch-Zener oscillations have been observed for light waves in waveguide arrays, while the phase coherence between interfering path has not been explicitly verified [8]. Stückelberg interference based on two partial Landau-Zener transitions has been observed with Rydberg atoms [9], superconducting systems [10, 11], and in ultracold molecular physics where this method was applied to measure Feshbach molecular levels [12]. Recent theoretical work has discussed the possibility to simulate quasirelativistic effects in a two-band cold atom system, which in the presence of interactions can be described by a nonlinear Dirac equation [13].

Here we report on the observation of Bloch-Zener oscillations with ultracold atoms in an optical lattice with a two-band miniband structure. We have also observed an interference signal based on two partial Landau-Zener transitions between Bloch bands of the optical lattice. From measured fringe patterns of this Stückelberg interferometer, the energetic splitting between the bands at an arbitrary value of the atomic quasimomentum can be determined. This realizes a novel method to interferometrically map out the band structure of an optical lattice.

Before proceeding, we note that band structure determinations have a long history in the solid state physics community, and powerful methods here include neutron scattering and both optical and X-ray spectroscopy [1]. For cold atoms in optical lattices, vibrational frequencies and the splitting between bands at the position of the gaps can be readily

determined by the well established techniques of parametric heating [14], Rabi-oscillations at the gaps [15] and Landau-Zener tunneling [16]. The full band structure of an optical lattice could in principle be determined by Bragg spectroscopy, but this requires a continuous change of the angle between the driving laser beams [17].

Our experiment uses lattice potentials realized by superimposing a conventional standing wave lattice potential of  $\lambda/2$  spatial periodicity with a  $\lambda/4$  periodicity lattice realized with the dispersion of a multiphoton Raman process [18, 19]. The splitting between the lowest energetic Bloch band and the first excited band is determined by first order Bragg scattering of the standing wave lattice potential, while the splitting between the first and the second excited band is due to the interference of contributions of second order Bragg scattering of the standing wave lattice potential and that of first order Bragg scattering of the fourth order ( $\lambda/4$ -spatial periodicity) lattice. By choosing a relatively large value of the amplitude of the multiphoton lattice potential, the splitting between the first and the second excited band can be made large so that the tunneling rate to higher bands is small. In this way, a miniband structure with two closely spaced subbands is prepared, in between the Landau-Zener tunneling rate is large. In the following,  $V_1$  and  $V_2$  denote the potential depths of the two lattice harmonics with spatial periodicities  $\lambda/2$  and  $\lambda/4$  respectively,  $\phi$  the relative phase between lattice harmonics, and  $k = 2\pi/\lambda$  is the optical wavevector. For a Fourier-synthesized lattice potential of the form  $V(z) = (V_1/2) \cos(2kz) + (V_2/2) \cos(4kz + \phi)$ , if  $\Delta_1$  and  $\Delta_2$  denote the splittings between the ground and the first excited band, and the first and the second excited band respectively (see Fig. 1a),  $\Delta_2$  is maximised for a relative phase between lattice harmonics of  $\phi = 0$  [19]. If  $\Delta_2 > \Delta_1$ , as is desirable when considering atom dynamics in the lowest two bands, the corresponding bands are commonly called minibands. In general, minibands emerge above a certain value of the ratio of the potential depth of the harmonics:  $V_2/V_1 > r(\phi, V_1, V_2)$ . Fig. 1a shows the calculated band structure of such a lattice for the experimental parameters used.

Our experiment starts with an atomic rubidium Bose-Einstein condensate loaded into a lattice at rest relatively to the rest frame of the atoms, so that atoms are transferred into the lowest energy band at a quasimomentum  $q(0) = 0$ . Subsequently, the lattice is accelerated relatively to the free falling atoms, which is equivalent to the application of an external force  $F$  to the atoms, and the quasimomentum evolves in time to larger quasimomenta, following  $q(t) = q(0) + F \cdot t$ . By the time that the atomic wavepacket reaches the first bandgap, part

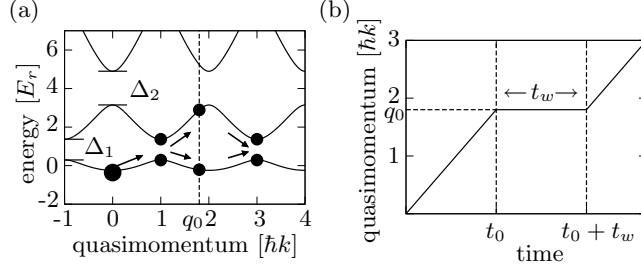


FIG. 1. (a) Band structure of the Fourier-synthesized optical lattice potential along with a scheme of the Stückelberg interferometer. In the lattice frame, atoms are accelerated over the first bandgap, where partial Landau-Zener tunneling creates a coherent superposition of wavepackets in the lowest two Bloch-bands. To induce a controllable phase shift between paths, the acceleration can be stopped at a quasimomentum  $q_0$  (with  $\hbar k \leq q_0 \leq 3\hbar k$ ) for a waiting time  $t_w$ . The acceleration then continues until this bandgap is again reached at a quasimomentum of  $3\hbar k$  to close the atom interferometer. The parameters used for the band structure were  $V_1 = 2.7 E_r$ ,  $V_2 = 3.2 E_r$ , and  $\phi = 0^\circ$ . (b) Variation of the quasimomentum with time for realizing the Stückelberg interferometer.

of the wavepacket experiences Landau-Zener tunneling through the gap into the first excited Bloch band, while the remaining part remains in the lowest band and is Bragg reflected. The corresponding beam splitting process is visualized in the extended band structure scheme shown in Fig. 1a. The splitting ratio can be controlled by tuning the size of the gap, which to lowest order is determined by the magnitude of  $V_1$ . In this way, a coherent superposition of wavepackets in the two different subbands of the miniband structure is created. To shift the relative phase between the two paths, the acceleration can be stopped at some value of the quasimomentum  $q_0$  (with  $q_0 = q(t_0)$  and  $\hbar k \leq q_0 \leq 3\hbar k$ ) for a waiting time  $t_w$ . We expect that the wavefunctions during this waiting time in the ground and first excited subbands then evolve as:

$$\begin{aligned}\psi_1(q_0, t) &= \psi_1(q_0, t_0) \exp(-E_1(q_0)(t - t_0)/\hbar), \\ \psi_2(q_0, t) &= \psi_2(q_0, t_0) \exp(-E_2(q_0)(t - t_0)/\hbar),\end{aligned}\tag{1}$$

where  $E_1(q_0)$  and  $E_2(q_0)$  denote the corresponding eigenenergies at a quasimomentum  $q_0$ , so that a relative phase between the subbands  $\Delta\varphi(q_0, t_0 + t_w) = [E_2(q_0) - E_1(q_0)]t_w/\hbar$  is accumulated in a time  $t_w$ . Subsequently, the acceleration is continued, and at a quasimomentum of  $3\hbar k$  in the extended band scheme of Fig. 1a we again reach the bandgap between the

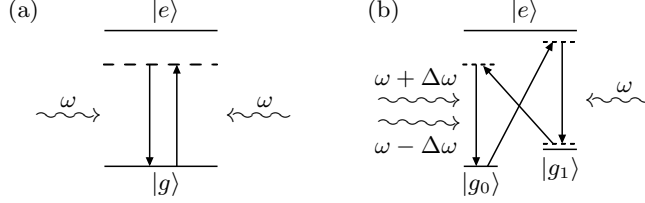


FIG. 2. (a) Virtual two-photon process in a standing wave lattice with  $\lambda/2$  spatial periodicity. (b) Virtual four-photon processes contributing to a lattice potential with  $\lambda/4$  spatial periodicity, as the higher harmonic of the used Fourier-synthesized lattice potential.

ground and the first excited Bloch band, where Landau-Zener tunneling acts as a second beam splitter to recombine the two wavepackets and close the atom interferometer.

The acceleration stops here at a quasimomentum of  $3\hbar k$  and the lattice is switched off, after which a time of flight image is recorded. Correspondingly, the lattice eigenstates at the position of the crossing are mapped onto the free atomic eigenstates. Depending on the relative phase between wavepackets, atoms at the interferometer output will either be transferred into the first or the second diffraction order in the far field image. As a function of the waiting time  $t_w$  in the acceleration sequence, we expect a sinusoidal fringe pattern oscillating between the two different lattice diffraction orders. Notably, as this fringe pattern oscillates at a frequency  $\omega = [E_2(q_0) - E_1(q_0)]/\hbar$ , the oscillation frequency allows to interferometrically determine the energetic splitting between ground and first excited band of the Bloch spectrum at a given value of the quasimomentum  $q_0$ . Fig. 1b shows a scheme of the variation of the lattice quasimomentum with time. It is clear that from a variation of the quasimomentum at which the acceleration is stopped, the complete spectrum  $\omega(q)$  of the miniband structure can be mapped out. We expect that this description is valid when the Landau-Zener tunneling rate into higher bands is small, as can be achieved for gap sizes  $\Delta_2 > \Delta_1$  in the miniband structure. Otherwise, we expect a reduced number of atoms at the interferometer output due to loss into other diffraction orders.

Bloch-Zener oscillations now refer to measurements where the relative phase between the path between wavepackets was left at a constant value, as can be reached by simply setting  $t_w = 0$ , (i.e. omitting the waiting time), and monitoring the populations in the different bands versus time. In this case, we expect that the mean atomic momentum performs a characteristic double periodic motion with the two Bloch periods  $T_B^{(1)} = 2\hbar k/F$

and  $T_B^{(2)} = 4\hbar k/F$  [4]. This corresponds to a coherent superposition of Bloch-oscillations and Landau-Zener tunneling in the two-miniband structure.

Our experimental setup used to investigate ultracold rubidium atoms in a Fourier-synthesized optical lattice is similar as described previously [20]. Briefly, an atomic rubidium ( $^{87}\text{Rb}$ ) Bose-Einstein condensate is produced all-optically by evaporative cooling of atoms in a CO<sub>2</sub>-laser dipole trap. In the final stages of evaporation, a magnetic field gradient is applied, and this results in a spin-polarized condensate with  $3 \cdot 10^4$  atoms in the  $m_F = -1$  component of the  $F = 1$  hyperfine ground state. The method used to produce a Fourier-synthesized optical lattice potential for the atoms [18], with which the described miniband structure can be achieved, is as follows. For the fundamental spatial frequency of periodicity  $\lambda/2$ , a usual standing wave lattice is used produced by two counterpropagating beams of frequency  $\omega$  (red detuned from an atomic resonance). The well known processes contributing in a quantum picture to this lattice potential arising from the spatially varying ac-Stark shift are indicated in Fig. 2a. A lattice potential of spatial periodicity  $\lambda/4$ , as the first harmonic for a Fourier-synthesis of lattice potentials, is produced with a multiphoton Raman technique. The scheme uses three-level atoms with two stable ground states  $|g_0\rangle$  and  $|g_1\rangle$  and one electronically excited state  $|e\rangle$ . The atoms are irradiated by two copropagating optical beams of frequency  $\omega + \Delta\omega$  and  $\omega - \Delta\omega$  respectively and a counterpropagating beam of frequency  $\omega$ , see Fig. 2b. During the induced virtual four-photon processes, the optical field exchanges momentum with the atoms in units of four photon recoils with the atoms, which is a factor two above the corresponding processes in a standing wave. The spatial periodicity of the induced four-photon lattice potential is  $\lambda/4$  [19]. In our experiment, the rubidium  $F = 1$  ground state Zeeman sublevels  $m_F = -1$  and  $0$  are used as levels  $|g_0\rangle$  and  $|g_1\rangle$ , and the  $5P_{3/2}$  manifold as the excited state  $|e\rangle$ . A homogeneous magnetic bias field of 1.8 G removes the degeneracy of the Zeeman sublevels. The light to generate the optical lattice potential is produced by a high power diode laser detuned 1 nm to the red of the rubidium D<sub>2</sub> line. The emitted beam is split into two, from which the two counter-propagating beams for generation of the periodic potential is derived. In each of the beams, an acoustooptic modulator generates all required optical frequencies in the corresponding beam path. The potential depths and the relative phase of the two spatial lattice harmonics can be controlled individually.

After preparation of the rubidium Bose-Einstein condensate, the CO<sub>2</sub>-laser trapping beam

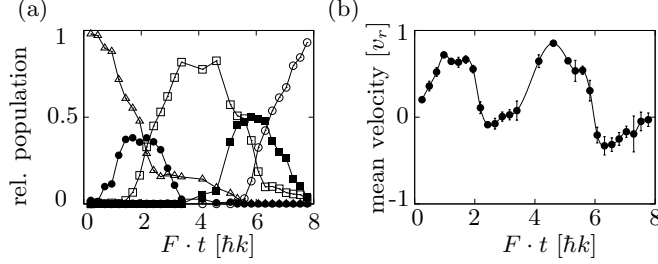


FIG. 3. Experimental data for Bloch-Zener oscillations of atoms in the biharmonic lattice potential, which was accelerated with a constant acceleration relatively to the atomic rest frame. (a) Relative population of diffraction orders versus time: zeroth order (triangles), first order (filled circles), second order (open squares), third order (filled squares), and fourth order (open circles) respectively. The solid line is to guide the eye. (b) Mean atomic velocity (circles) in the co-moving frame versus time, where  $v_r = \hbar k/m$  denotes the recoil velocity and  $m$  the atomic mass. The solid line is a spline fit.

is extinguished, leaving the atoms in ballistic free fall. The vertically oriented lattice beams are activated 2.5 ms after the release of the condensate from the trap, so that due to the lowering of the density during expansion the interatomic interactions are reduced. During the free fall of the atoms, the lattice beams are initially switched on to adiabatically load the atoms into the lowest band of the Fourier-synthesized lattice at  $q = 0$ . For a measurement of Bloch-Zener oscillations one of the lattice beams (the beam shown on the right side of Figs. 2a and 2b) is subsequently acousto-optically detuned with a constant chirp-rate to accelerate the lattice with respect to the atomic rest frame. Note that a tuning of this beam's frequency moves both the  $\lambda/2$  and the  $\lambda/4$  spatial component in a phase-stable way, so that the shape of the lattice is not affected by the acceleration sequence. For the shown experimental data the depths of the lattice harmonics were  $V_1 = 2.7 E_r$  and  $V_2 = 3.2 E_r$ , where  $E_r = (\hbar k)^2/2m$  denotes the recoil energy, the relative phase between the harmonics was  $\phi = 0^\circ$ . The acceleration used in the atomic frame was  $25 \text{ m/s}^2$ . Fig. 3a shows the measured relative populations of the different diffraction orders of the lattice after a variable acceleration time  $t$ . The data allows to follow the wavepacket motion in the miniband Bloch band structure (see Fig. 1a) in time. When  $F \cdot t \approx \hbar k$ , the band gap between the ground band and the first excited Bloch band is reached, resulting a subsequent decrease of the observed population of the zeroth diffraction order (data with triangles) and an increase of the population of

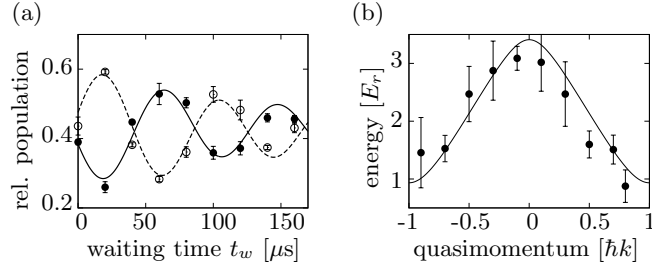


FIG. 4. (a) Measured Stüeckelberg interference fringes based on two partial Landau-Zener transitions between the bandgaps of the optical lattice. The filled (open) circles give the measured relative population in the first (second) diffraction respectively versus the waiting time  $t_w$ , with  $q_0 = 1.9 \hbar k$  for this data set. The dashed and solid lines are fits to the data. (b) The data points give the interferometrically determined energy difference between the two minibands versus the lattice quasimomentum in the atomic frame. The solid line is the calculated energy difference.

the first diffraction order to roughly 40% (filled circles), which is attributed to the partial Landau-Zener tunneling into the first excited Bloch band. Note that the splitting at this band gap does not exactly match a 50/50 ratio. When  $F \cdot t \approx 2\hbar k$ , the zero's order peak is Bragg deflected into the second order peak (data with open squares), i.e. only the mapping onto the free eigenstates charges, while when  $F \cdot t \approx 3\hbar k$  is reached again a partial Landau-Zener transition occurs with the relative phase between wavepackets being such that most of the population is transferred into the lowest energy band, which after crossing maps onto the second diffraction order, and the observed corresponding relative population then increases to roughly 85%. We attribute the difference to 100% as being mainly due to partial Landau-Zener tunneling into higher bands. For larger times, a second cycle of the wavepacket motion in the miniband structure is observed. We attribute the corresponding data as evidence for Bloch-Zener oscillations in the Fourier-synthesized optical lattice. Fig. 3b gives the mean velocity of the atoms in the co-accelerated frame versus time, as derived from the data of Fig. 3a.

Fig. 4a shows data where the relative phase was varied between the two interfering paths of the formed Landau-Zener-Stüeckelberg band interferometer. For the corresponding measurement, the acceleration sequence was stopped after the first beam splitting process at a certain value of the quasimomentum  $q_0$  (with  $q_0 = 1.9\hbar k$  for the here shown data) for a variable waiting time to induce a variable phase shift. The filled (open) circles in Fig. 4a give



the measured population in the first (second) order Bragg peak after releasing the condensate from the lattice when reaching a quasimomentum of  $3\hbar k$ . As a function of the waiting time  $t_w$ , which due to the energy difference of the two bands tunes the accumulated relative phase, a clear interference pattern in the relative population of Bloch bands is observed at the interferometer output. From the measured oscillation frequency, the energy difference between the Bloch bands at the corresponding quasimomentum can readily be determined. We attribute the observed damping of the fringe signal for large times  $t_w$  to the finite velocity spread of atoms after their release from the trap. By the time of the experiment, the condensate interaction energy has been converted into kinetic energy. The corresponding velocity spread is expected to cause a nonzero width of the quasimomentum distribution in the lattice. This will lead to a spread of oscillation frequencies of the Stückelberg interference signal, and a corresponding loss of contrast for larger times  $t_w$ . The solid and dashed lines in Fig. 4a are fits to the experimental fringe signal with a convolution of sinusoidal curves to account for the loss of contrast for larger times  $t_w$  (for a measured atomic velocity spread of  $\pm 0.8\hbar k$  for this data set). We note that in a quantum simulations view of our two-bands Bloch structure experiment, the observed oscillation frequency can be interpreted as a beating occurring at the Zitterbewegung frequency [21, 22]. Fig. 4b shows the derived energy splitting between the ground and the first excited Bloch band of the miniband structure as a function of the quasimomentum for the complete Brillouin zone. The solid line is the theoretically expected curve of the energy difference for the given experimental parameters of the potential depths and relative phase of lattice harmonics, which is in good agreement with the corresponding experimental values. The smaller variation of the measured energy difference over the Brillouin zone with respect to the theoretical curve is attributed to the nonzero atomic velocity spread.

To conclude, we have observed Bloch-Zener oscillations in an optical lattice using a miniband-type Bloch band structure. The relative phase of wavepackets in different Bloch bands was varied, which has allowed to demonstrate the coherence of the formed Landau-Zener interferometer and demonstrate a novel method to interferometrically map out the energy difference between bands over the complete Brillouin zone.

We expect that the described method has prospects for precise interferometric determinations of the band structure in optical lattices. The velocity spread of the atoms can be reduced by Raman selection [23]. In principle, the method should also be applicable

to usual standing wave lattices when during the acceleration sequence the Landau-Zener tunneling rate between Bloch bands is tailored dynamically either by appropriate variation of the potential depth of the lattice, similar as described in [24], or by variation of the acceleration rate with time. For example, when the ramp speed is correspondingly reduced in the vicinity of the crossing between the first two excited bands, the tunneling rate to higher bands can be kept small. Other prospects of the discussed coherent manipulation in the miniband structure can include quantum simulations of the (linear and nonlinear) Dirac equation [22]. The described interferometric method may also be used to test for deviations of Newton's law over microscopic distances, in a spirit similar than earlier experiments based on Bloch-oscillations [25].

We thank D. Witthaut for helpful discussions. Financial support from the Deutsche Forschungsgemeinschaft is acknowledged.

- 
- [1] see e.g. N. W. Ashcroft and N. D. Mermin, *Solid State Physics* (Saunders College Publishing, New York, 1976).
  - [2] J. Feldmann, K. Leo, J. Shah, D. A. B. Miller, J. E. Cunningham, T. Meier, G. von Plessen, A. Schulze, P. Thomas, and S. Schmitt-Rink, *Phys. Rev. B* **46**, 7252 (1992).
  - [3] M. Ben Dahan, E. Peik, J. Reichel, Y. Castin, and C. Salomon, *Phys. Rev. Lett.* **76**, 4508 (1996).
  - [4] B. M. Breid, D. Witthaut, and H. J. Korsch, *New J. Phys.* **8**, 110 (2006).
  - [5] B. M. Breid, D. Witthaut, and H. J. Korsch, *New J. Phys.* **9**, 62 (2007).
  - [6] E. C. G. Stückelberg, *Helv. Phys. Acta* **5**, 369 (1932).
  - [7] E. E. Nikitin and S. Y. Umanskii, *Theory of Slow Atomic Collisions* (Springer, Heidelberg, 1984).
  - [8] F. Dreisow, A. Szameit, M. Heinrich, T. Pertsch, S. Nolte, A. Tünnermann, and S. Longhi, *Phys. Rev. Lett.* **102**, 076802 (2009).
  - [9] S. Yoakum, L. Sirko, and P. M. Koch, *Phys. Rev. Lett.* **69**, 1919 (1992).
  - [10] W. D. Oliver, Y. Yu, J. C. Lee, K. K. Berggren, L. S. Levitov, and T. P. Orlando, *Science* **310**, 1653 (2005).
  - [11] M. Sillanpää, T. Lehtinen, A. Paila, Y. Makhlin, and P. Hakonen, *Phys. Rev. Lett.* **96**, 187002

- (2006).
- [12] M. Mark, T. Kraemer, P. Waldburger, J. Herbig, C. Chin, H. C. Nägerl, and R. Grimm, *Phys. Rev. Lett.* **99**, 113201 (2007).
  - [13] M. Merkl, A. Jacob, F. E. Zimmer, P. Öhberg, and L. Santos, *Phys. Rev. Lett.* **104**, 073603 (2010).
  - [14] S. Friebel, C. D’Andrea, J. Walz, M. Weitz, and T. W. Hänsch, *Phys. Rev. A* **57**, 20 (1998).
  - [15] A. S. Mellish, G. Duffy, C. McKenzie, R. Geursen, and A. C. Wilson, *Phys. Rev. A* **68**, 051601 (2003).
  - [16] O. Morsch and M. Oberthaler, *Rev. Mod. Phys.* **78**, 179 (2006).
  - [17] D. Clément, N. Fabbri, L. Fallani, C. Fort, and M. Inguscio, *Phys. Rev. Lett.* **102**, 155301 (2009).
  - [18] G. Ritt, C. Geckeler, T. Salger, G. Cennini, and M. Weitz, *Phys. Rev. A* **74**, 063622 (2006).
  - [19] T. Salger, C. Geckeler, S. Kling, and M. Weitz, *Phys. Rev. Lett.* **99**, 190405 (2007).
  - [20] G. Cennini, G. Ritt, C. Geckeler, and M. Weitz, *Phys. Rev. Lett.* **91**, 240408 (2003).
  - [21] J. Y. Vaishnav and C. W. Clark, *Phys. Rev. Lett.* **100**, 153002 (2008).
  - [22] R. Gerritsma, G. Kirchmair, F. Zähringer, E. Solano, R. Blatt, and C. F. Roos, *Nature* **463**, 68 (2010).
  - [23] M. Kasevich and S. Chu, *Phys. Rev. Lett.* **67**, 181 (1991).
  - [24] A. Zenesini, H. Lignier, G. Tayebirad, J. Radogostowicz, D. Ciampini, R. Mannella, S. Wimberger, O. Morsch, and E. Arimondo, *Phys. Rev. Lett.* **103**, 090403 (2009).
  - [25] G. Ferrari, N. Poli, F. Sorrentino, and G. M. Tino, *Phys. Rev. Lett.* **97**, 060402 (2006).